Available online at www.sciencedirect.com
SCIENCE DIRECT®
PERGAMON
International Journal of Heat and Mass Transfer 46 (2003) 4863–4875
International Journal of HEAT and MASS TRANSFER
www.elsevier.com/locate/ijhmt

Non-Darcian thermal stability of a heat generating fluid in a porous annulus

S. Saravanan [a], P. Kandaswamy [b,*]

[a] Department of Mathematics and Computer Applications, Kumaraguru College of Technology, Coimbatore 641 006, Tamil Nadu, India
[b] Department of Mathematics, Bharathiar University, Coimbatore 641 046, Tamil Nadu, India

Received 26 July 2002; received in revised form 2 May 2003

Abstract

A linear stability analysis has been implemented for a viscous flow induced by internal heat sources in a vertical annular porous region bounded by two concentric cylinders. The analysis is made under the assumption that the flow is parallel to the cylinders. The perturbation equations are solved by a Chebyshev collocation spectral method. Results are given for a wide range of gaps. The critical curves in several planes formed by the physical parameters of the problem are plotted. In particular, the effects of the porous parameter and the radius ratio are examined.

1. Introduction

Nuclear energy continues to attract scientists though they are examining various means to produce energy. But the accidents that may occur in nuclear reactors pose a severe problem to them. In the risk assessment of nuclear power plants, the possibility and the consequences of a melt escaping from the core are usually considered. During the course of an accident, molten fuel may interact with coolant, and get converted into fine particles because of some thermal reactions. These small particles quickly solidify in the coolant and settle on the internal structure forming a saturated porous particle bed. Fixed porous beds are also used as the basis for reacting systems in certain reactors such as tubular bed reactor and packed bed enzyme reactor. Hence a thorough understanding of heat and mass transfer in porous media and their stability, arising because of volumetric energy sources has become an important issue especially in nuclear [1–3] and chemical engineering [4,5].

When a fluid permeates a porous medium, the actual path of an individual particle cannot be followed analytically. The gross effect must be represented by a macroscopic law relating the fluid flux and the dimensions of porous structure which is the Darcy law. It applies to unidirectional flow in an unbounded porous medium. It does not account for inertial and boundary effects that become important when the flow is curvilinear and near a solid surface. But it is well known that the curvature of the fluid path gives rise to inertial acceleration. This drawback was eliminated by Lapwood [6] after his generalization of Darcy's law in the form

$$\rho\left(\frac{\partial \bar{v}^*}{\partial t^*} + (\bar{v}^* \cdot \nabla^*)\bar{v}^*\right) = -\nabla^* p^* + \rho \bar{g} - \frac{\mu}{K}\bar{v}^* \tag{1}$$

which we call as Darcy–Lapwood (DL) equation. Moreover if a high-porosity medium is bounded by an impermeable solid surface the resistance offered by it to the flow should be included in addition to Darcy friction. Hence the viscous resistance $\mu_e(\nabla^*)^2\bar{v}^*$ was included [7] to the form

$$\rho\left(\frac{\partial \bar{v}^*}{\partial t^*} + (\bar{v}^* \cdot \nabla^*)\bar{v}^*\right) = -\nabla^* p^* + \rho \bar{g} - \frac{\mu}{K}\bar{v}^* + \mu_e(\nabla^*)^2\bar{v}^* \tag{2}$$

* Corresponding author. Tel.: +91-422-422222; fax: +91-422-422387.
E-mail addresses: sshravan@lycos.com (S. Saravanan), pgk0@lycos.com (P. Kandaswamy).

0017-9310/$ - see front matter © 2003 Elsevier Ltd. All rights reserved.
doi:10.1016/S0017-9310(03)00333-8

Nomenclature

c_p	specific heat capacity
Da	Darcy number
g	acceleration due to gravity
Gr	Grashof number
k	wavenumber
K	permeability
$\hat{k}$	unit vector in the z direction
n	number of collocation points
p	pressure
Pr	Prandtl number
q	$Q_m/((\rho c_p)_f \kappa_f)$
Q_m	volume density of internal heat sources
r	radial coordinate
R	radius ratio
r_1, r_2	nondimensional radii of inner and outer cylinders
R_1, R_2	radii of inner and outer cylinders
t	nondimensional time
T	nondimensional temperature
$\bar{v}$	nondimensional velocity vector
x	$r - \frac{1+R}{1-R}$
z	vertical coordinate

Greek symbols

β	coefficient of thermal expansion
κ	thermal diffusivity
λ	complex eigenvalue
μ	viscosity
μ_e	effective viscosity
$\bar{\mu}$	viscosity ratio
ν	kinematic viscosity
ρ	density
σ	porosity parameter
Ω	heat capacity ratio
Ψ	nondimensional stream function
∇	Laplacian operator

Superscripts

*	dimensional quantity
(i)	ith derivative

Subscripts

c	critical state
m	porous medium comprising fluid and solid phases
f	fluid phase
0	basic state

which reduces, for steady Reynolds number flow to one proposed by Brinkman [8] for creeping flow. Here μ_e denotes the effective viscosity of fluid based on a volume-averaging process in interconnected pores. Hereafter we will call (2) as Darcy–Lapwood–Brinkman (DLB) equation. This model is flexible in the sense that it has a parameter K, the permeability, such that it reduces to a form of Navier–Stokes equation as $K/L^2 \to \infty$ and the Darcy's law as $K/L^2 \to 0$ where L is the characteristic macroscopic length scale. For sufficiently large fluid velocities the form drag due to the presence of solid obstacles becomes comparable with the surface drag due to friction. This introduces a quadratic drag as pointed out by Forchheimer. But the present work is merely intended to give some light on the hydrodynamical stability properties of flow through porous media. Moreover there is some uncertainity about the validity of DLB model with Forchheimer correction at large porosity (see [9]). Hence the quadratic drag is neglected and the entire work is based on DLB model.

Thermal convection of a fluid contained between two vertical walls kept at different isothermal temperatures is one of the typical convection systems with simple geometrical and thermal constraints. The situation becomes entirely different when the motion is induced because of uniformly distributed internal heat sources with isothermal walls. It has not been well studied as that of the differential heating counterpart. In this case two counter-rotating vortices are formed because of the underlying even parabolic temperature profile. Also the transition from stationary to oscillatory mode of instability becomes continuous. When the curvature effect is included, this even temperature profile gets skewed towards the inner wall. This converts the vortices into a single chain of eddies originating near the inner wall. Much of the work on natural convection because of internal heat sources has been concerned with porous layer between two planes [9]. Only in the last two decades, the authors have started investigating other types of porous configurations, particularly cylindrical enclosures.

Stewart and Dona [10] considered free convection in a closed finite vertical porous cylinder and found that the isotherms were compressed near the top and side walls of the cylinder as Rayleigh number is increased. Their work was extended to an aspect ratio of 20 by Prasad and Chui [11] in a Darcy porous medium. Farr et al. [12] studied the stability of an exothermic reaction driven convection in a Darcy porous medium contained in a closed vertical cylinder. They found that the onset of convection has a threshold Ra as the Frank Kamenetskii parameter is increased from zero to the ignition point. Vasseur et al. [13] discussed convection in an annular porous layer between horizontal concentric cylinders.

Their calculations showed that, at large *Ra* values the flow structure consists of a thermally stratified core and two boundary layers. Numerical study of two-dimensional convection in a horizontal annulus filled with porous material in the presence of a permeable boundary was treated by Stewart and Burns [14]. Convective heat transfer in a packed vertical tube with axial and radial dispersions was studied by Adnani et al. [15].

A conducted literature survey indicates no work reporting convection in a heat generating fluid and its observability in an annular geometry with variable curvature. The earlier studies by Shikhov and Yakushin [16] and Kolyshkin and Vaillancourt [17] regarding the nonuniformity of heat sources have shown that curvature could substantially affect the critical boundary. Hence the purpose of the present work is to investigate the stability of natural convection in a vertical annular porous layer confined between two concentric vertical cylinders with special reference to curvature which has some important applications to the core-melt formation problem discussed earlier.

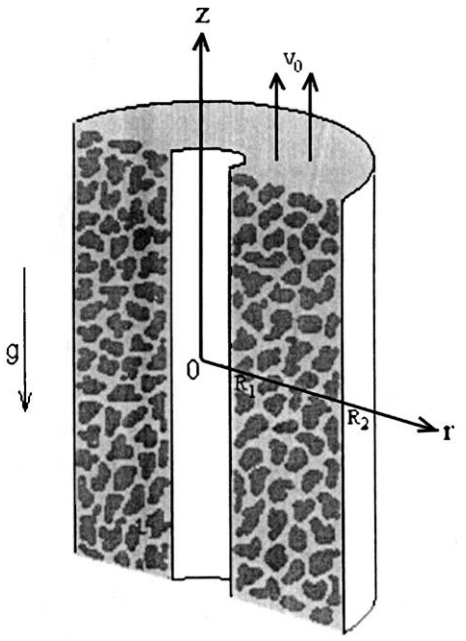

Fig. 1. A diametral cross-section of the physical configuration.

2. The equations

Let us consider a sparsely packed isotropic and homogeneous porous layer saturated with a viscous incompressible fluid. The layer is confined between two vertical long concentric cylinders of radii R_1 and R_2 ($R_1 < R_2$). The temperature of both the cylinder walls are kept constant and equal, which is taken as the reference point. We choose a cylindrical polar coordinate system, where the z-axis is directed opposite to gravity $\bar{g}$ (Fig. 1). The origin of the coordinate system is located in the cylinders' axis. The fluid is heated by uniformly distributed heat sources of volume density Q_m throughout the layer where the subscript m refers to overall medium comprising both solid and fluid phases. Further it is assumed that both the fluid and solid phases do remain in local thermal equilibrium. All the physical characteristics are taken as constant, except the density which varies linearly with temperature in the buoyancy term (Boussinesq approximation).

The equations governing the motion of a viscous incompressible fluid in the above configuration under Boussinesq approximation are

$$\rho\left(\frac{\partial \bar{v}^*}{\partial t^*} + (\bar{v}^* \cdot \nabla^*)\bar{v}^*\right) = -\nabla^* p^* - \frac{\mu}{K}\bar{v}^* + \mu_e(\nabla^*)^2\bar{v}^* + g\beta T^*\hat{k} \tag{3}$$

$$(\rho c)_m \frac{\partial T^*}{\partial t^*} + (\rho c_p)_f(\bar{v}^* \cdot \nabla^*)T^* = k_m(\nabla^*)^2 T^* + Q_m \tag{4}$$

$$\operatorname{div} \bar{v}^* = 0 \tag{5}$$

where $\bar{v}^*$ is the velocity of the fluid; T^*, the temperature; p^*, the pressure; K, the permeability of the porous medium and $\hat{k}$, the unit vector along the z-axis.

We define $h = (R_2 - R_1)/2$, $R = R_1/R_2$, $r_1 = 2R/(1-R)$, $r_2 = 2/(1-R)$ and introduce the nondimensional variables $r = r^*/h$, $z = z^*/h$, $t = t^*/(h^2/\nu)$, $\bar{v} = \bar{v}^*/(g\beta q h^4/2\nu)$, $p = p^*/(\rho g \beta h^3/2)$, $T = T^*/(qh^2/2)$. Let $q = Q_m/((\rho c_p)_f \kappa_f)$, $Gr = g\beta q h^5/2\nu^2$ be the Grashof number, $Pr_m = k_m/((\rho c_p)_f)\nu$ the Prandtl number, $\sigma = h/\sqrt{K}$ the porosity parameter, $\bar{\mu} = \mu_e/\mu$ the ratio of viscosities and $\Omega = (\rho c)_m/(\rho c_p)_f$ the heat capacity ratio. In dimensionless variables, Eqs. (3)–(5) become

$$\frac{\partial \bar{v}}{\partial t} + Gr(\bar{v} \cdot \nabla)\bar{v} = -\nabla p - \sigma^2 \bar{v} + \bar{\mu}\nabla^2 \bar{v} + T\hat{k} \tag{6}$$

$$\Omega \frac{\partial T}{\partial t} + Gr(\bar{v} \cdot \nabla)T = \frac{1}{Pr_m}\nabla^2 T + \frac{2}{Pr_m} \tag{7}$$

$$\operatorname{div} \bar{v} = 0 \tag{8}$$

Since our interest is a fluid saturated sparsely packed porous medium, Ω can be assumed, with sufficient accuracy, to be one. We seek a steady parallel solution for Eqs. (6)–(8) of the following type:

$$\bar{v} = [0, 0, v_0(r)], \quad T = T_0(r), \quad p = p_0(z) \tag{9}$$

The flow (9), may be realized in the middle portion of a sufficiently long vertical layer of fluid filled porous medium where the end effects are negligible. Substituting (9) into Eqs. (6)–(8) leads to the system

$$\frac{d^2v_0}{dr^2}+\frac{1}{r}\frac{dv_0}{dr}-\frac{\sigma^2}{\bar{\mu}}v_0=\frac{1}{\bar{\mu}}(D-T_0) \tag{10}$$

$$\frac{d^2T_0}{dr^2}+\frac{1}{r}\frac{dT_0}{dr}=-2 \tag{11}$$

where D is the separation constant. σ is related to the Darcy number, Da $(=\bar{\mu}K/h^2)$ by $Da=\bar{\mu}/\sigma^2$. The corresponding boundary conditions are

$$v_0(r_i)=0,\quad T_0(r_i)=0,\qquad i=1,2 \tag{12}$$

The solution at the basic state is given by

$$T_0(r)=-\frac{r^2}{2}+A\log r+B \tag{13}$$

$$v_0(r)=\sum_{i=1}^{\infty}c_i(r-\bar{r})^i \tag{14}$$

where

$$A=-\frac{r_2^2-r_1^2}{2\log R},\quad B=\frac{r_2^2}{2}-A\log r_2\quad\text{and}\quad \bar{r}=\frac{r_1+r_2}{2}$$

An approximation to (14) is obtained with the first five terms (up to $i=4$) as $v_0(x)$ for $R=0.8$ approach the velocity profile arising between two planes reported in our previous work [20] and the truncated terms produce no significant effect. The explicit expressions for c_i's ($i=0$–4) are too lengthy and are provided in Appendix A.

We consider the case of a closed channel. This warrants the fluid flow through the cross-section of the channel to be zero and hence

$$\int_{r_1}^{r_2}rv_0(r)\,dr=0 \tag{15}$$

The basic velocity profiles for different values of σ are shown in Fig. 2 in terms of the coordinate

$$x=r-\frac{1+R}{1-R} \tag{16}$$

It is seen that σ retards the basic flow and distorts it slightly. Also as the spacing between the cylinders becomes smaller, the velocity profile becomes almost symmetric with an upflow at the centre and two downflows near the boundaries of the channel.

We consider the stability of the basic state by the method of small perturbations. Let us consider the perturbed motion $\bar{v}_0+\bar{v}$, T_0+T, and p_0+p, where $\bar{v}$, T and p are small unsteady perturbations, $\bar{v}_0=v_0\hat{k}$. Let us assume that the perturbed quantities do not depend on the azimuthal direction (so-called axisymmetric perturbations). Then Eqs. (6)–(8) for the above perturbed state after linearization take the form:

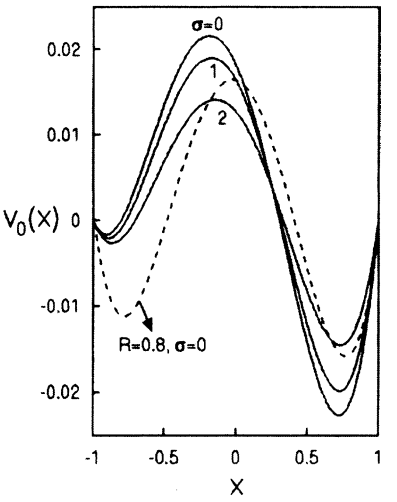

Fig. 2. Basic velocity profiles for different σ when $\bar{\mu}=1$ and $R=0.4$.

$$\frac{\partial\bar{v}}{\partial t}+Gr[(\bar{v}_0\cdot\nabla)\bar{v}+(\bar{v}\cdot\nabla)\bar{v}_0]=-\nabla p-\sigma^2\bar{v}+\bar{\mu}\nabla^2\bar{v}+T\hat{k} \tag{17}$$

$$\frac{\partial T}{\partial t}+Gr[(\bar{v}_0\cdot\nabla)T+(\bar{v}.\nabla)T_0]=\frac{1}{Pr_m}\nabla^2T \tag{18}$$

$$\operatorname{div}\bar{v}=0 \tag{19}$$

It is convenient to introduce the stream function $\Psi(r,z)$ as

$$v_r=-\frac{1}{r}\frac{\partial\Psi}{\partial z},\quad v_z=\frac{1}{r}\frac{\partial\Psi}{\partial x} \tag{20}$$

We set

$$\begin{aligned}\Psi(r,z,t)&=\phi(r)\exp(-\lambda t+ikz)\\ T(r,z,t)&=\theta(r)\exp(-\lambda t+ikz)\end{aligned} \tag{21}$$

where ϕ and θ are the amplitudes of the normal perturbations; k, the wavenumber and λ, a complex eigenvalue. Substituting (21) in Eqs. (17)–(19), we obtain the amplitude equations

$$\begin{aligned}L_1\phi=&\frac{\sigma^2}{\bar{\mu}}\left(\phi^{(2)}-\frac{1}{r}\phi^{(1)}-k^2\phi\right)+2k^2\phi^{(2)}-\frac{2k^2}{r}\phi^{(1)}\\&+\left(\frac{k^2}{r^2}-k^4\right)\phi+\frac{ikGr}{\bar{\mu}}\left(v_0\left(\phi^{(2)}-\frac{1}{r}\phi^{(1)}-k^2\phi\right)\right.\\&\left.+\phi\left(\frac{v_0^{(1)}}{r}-v_0^{(2)}\right)\right)-\frac{r}{\bar{\mu}}\theta^{(1)}-\frac{\lambda}{\bar{\mu}}\left(\phi^{(2)}-\frac{1}{r}\phi^{(1)}-k^2\phi\right)\end{aligned} \tag{22}$$

$$L_2\theta=k^2\theta+ikGrPr_m\left(v_0\theta-\frac{T_0^{(1)}}{r}\phi\right)-\lambda Pr_m\theta \tag{23}$$

where

$$L_1 = \left(r\frac{\mathrm{d}}{\mathrm{d}r}\left(\frac{1}{r}\frac{\mathrm{d}}{\mathrm{d}r}\right)\right)^2, \quad L_2 = \frac{1}{r}\frac{\mathrm{d}}{\mathrm{d}r}\left(r\frac{\mathrm{d}}{\mathrm{d}r}\right)$$

The velocity and temperature perturbations vanish at the sidewalls and hence the boundary conditions are

$$\phi(r_i) = 0, \quad \phi^{(1)}(r_i) = 0, \quad \theta(r_i) = 0, \qquad i = 1, 2 \qquad (24)$$

3. Method of solution

We solve the boundary value problem using the spectral collocation method based on the roots of Chebyshev polynomials which was successfully implemented in our previous study [20]. To locate an extremal point we proceed as follows. For fixed values of the other parameters, we determine the Grashof number $Gr(k)$ as a function of the wavenumber k corresponding to the case $Re(\lambda) = 0$. Then the critical Grashof number is found by setting $Gr_c = \min_k Gr(Pr_m, \bar{\mu}, R)$. The convergence of the numerical solution has been checked by varying the number of collocation points n. Table 1 shows the critical states for different combinations. We noticed that at $n = 13$ the 2% convergence criterion is met. Further increase in n considerably increases the cost. So we fixed n as 13 in our calculations. In addition to ensure that the errors in eigenvalue computations are minimal for all the cases considered, we defined a performance index P (see [18]) as

$$P = \max_{1 \leqslant i \leqslant n} \|\lambda_{Bi}\mathbf{A}.\mathbf{u}^i - \lambda_{Ai}\mathbf{B}.\mathbf{u}^i\| \times [(|\lambda_{Bi}|\|\mathbf{A}\|\|\mathbf{u}^i\| + |\lambda_{Ai}|\|\mathbf{B}\|\|\mathbf{u}^i\|)\epsilon]^{-1} \qquad (25)$$

Here $\lambda_i = \lambda_{Ai}/\lambda_{Bi}$ and u^i are the associated eigensystem. The quantity ϵ specifies the relative precision of the real variable, 10^{-8} in the present case. The notations $|\cdot|$ and $\|\cdot\|$ are used to represent respectively, the norm of a vector and the row sum norm of a matrix. When P is less than unity, the performance of the eigensystem code is considered to be excellent in the sense that the residuals $(\lambda_B\mathbf{A}.\mathbf{u} - \lambda_A\mathbf{B}.\mathbf{u})$ can be made as small as possible. We monitored the value of P and kept it below 0.8.

4. Results and discussion

Before discussing the stability phenomena, it is of interest to compare our results with previous stability solutions. Table 2 presents a comparison between published critical conditions and the numerical values of the present investigation, at various Prandtl numbers. Gershuni et al. [19] used approximating polynomials of different lengths in their Galerkin's method and so their results differ slightly. Still we observe a good agreement between the results at the same conditions which provide a further check on the numerical accuracy.

Computations were carried out for a wide range of parameters of the problem and the numerical results are presented to illustrate the effect of each controlling parameter. Several combinations of parameters in the range $0 \leqslant Gr \leqslant 20,000$, $0.01 \leqslant Pr \leqslant 10$ and $0.01 \leqslant R \leqslant 0.8$ are considered. The value of Darcy number for many porous materials is low. However, recently Weinert and Lage (see [9]) reported a sample of hyperporous compressed aluminium foam for which Da was about 8. Hence to get a more general theoretical insight, we fixed the range of σ as $0 \leqslant \sigma \leqslant 5$. Givler and Altobelli (see [9])

Table 1
Critical Grashof numbers for different n ($\Omega = \bar{\mu} = 1$)

n	$R = 0.1, \sigma = 1, Pr_m = 5$	$R = 0.2, \sigma = 5, Pr_m = 1$	$R = 0.5, \sigma = 3, Pr_m = 5$	$R = 0.7, \sigma = 1, Pr_m = 1$
7	738.75	3738.16	543.93	744.66
10	650.94	6549.99	631.56	817.75
11	622.81	5906.94	686.24	854.50
12	608.28	5595.55	710.58	842.87
13	602.16	5527.04	713.26	831.65

Table 2
Comparison of the present results for $n = 13, \Omega = 1, \bar{\mu} = 1$ and $\sigma = 0$ with others

R	Pr_m	Gr_c	k_c	c_c
0.9 (results of Gershuni et al. [19] within braces)	0.01 (0)	1674.15 (1720)	2.01 (2.05)	−0.21 (−0.16)
	1	731.52 (744)	1.35 (1.38)	−0.98 (−0.87)
	5	254.04 (259)	1.32 (1.35)	−1.36 (−1.21)
	20	113.85 (115)	1.34 (1.40)	−1.52 (−1.36)
0.7 (results of Kolyshkin and Vaillancourt [17] within braces)	5	260.02 (262.4)	1.25 (1.33)	−1.23 (−1.18)
	20	115.89 (116.4)	1.29 (1.37)	−1.40 (−1.33)

matched theoretical and observed velocity profiles for a rigid foam of porosity 0.972 and observed a value of about 7.5 for $\bar{\mu}$. This result motivated us to vary $\bar{\mu}$ in the interval [1,5].

In the discussion to follow, we fixed $\bar{\mu}$ as 1. We notice that the shape of the marginal stability curves change considerably if some of the parameters are changed. The effect of Pr_m on the marginal stability curve for a clear fluid ($\sigma = 0$) is shown in Fig. 3. For a low Pr_m approximation (i.e., at $Pr_m = 0.01$), the neutral curve A has a single minimum. Since the low Prandtl number fluids are good conductors of heat, they immediately dissipate the temperature disturbances before the disruption of buoyancy force to cause instability. Hence the instability causing the single minimum by the unstable velocity distribution is referred to as shear (S) mode.

On the other hand as Pr_m increases, the penetration depth of temperature disturbances decreases, and hence the buoyant force becomes more concentrated resulting in an instability. In Fig. 4 we see that the critical Grashof number Gr_c is considerably lowered with a corresponding shift towards the lower wavenumber region even for $Pr_m = 1$. Further increase in Pr_m results in the development of a nose shaped piece, labelled as B, in the curve in the lower wavenumber region. This converts the neutral curve into two branches, having a local minimum in each branch separated by a local maximum. Hence the nose shaped part of neutral curve represents the difference between full stability problem and the Orr–Sommerfeld problem for the same velocity profiles. Accordingly the marginal wavespeed becomes bimodal as shown in Fig. 3. The wavespeed is measured in the same units as the velocity of the base flow and is normalized by the modulus of maximum velocity of base flow: $c = \mathrm{Im}(\lambda)/(k\,Gr\,v_{0\max})$, where λ is a purely imaginary eigenvalue and $v_{0\max}$, the absolute value of the maximum nondimensional velocity. Perturbations in the form of thermal running waves with comparatively high phase velocity correspond to the nose shaped lower part, and hence this branch is associated with thermal–buoyant (TB) mode of instability.

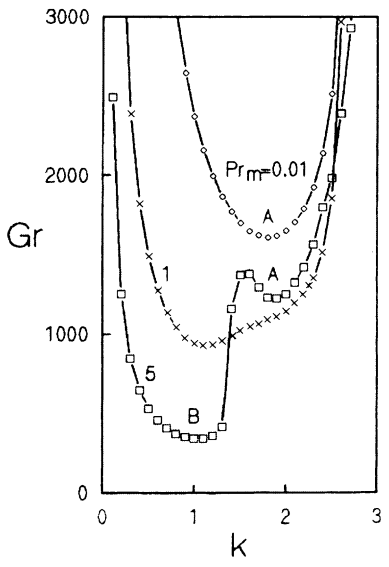

Fig. 3. Marginal stability curves for different Pr_m when $\bar{\mu} = 1$, $R = 0.4$ and $\sigma = 0$.

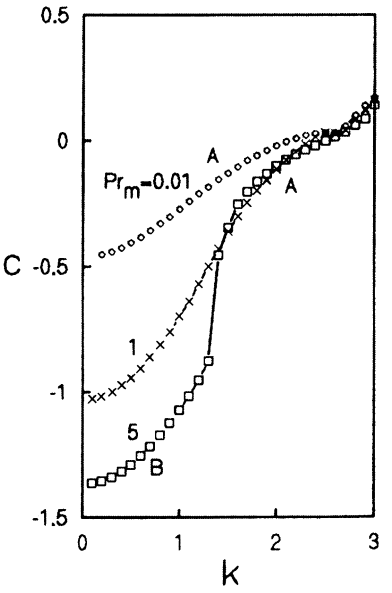

Fig. 4. Marginal wavespeeds for different Pr_m when $\bar{\mu} = 1$, $R = 0.4$ and $\sigma = 0$.

Now we shall investigate the effect of Darcy friction for an annular porous medium of $R = 0.4$. The marginal curve (Fig. 5) has two branches A and B corresponding to the S and TB modes, as discussed earlier. When σ becomes 1, the branch A is comparatively displaced more upwards indicating less contribution of shearing force to the instability mechanism. A further increase in σ together with Fig. 6 shows that the TB mode plays a vital role and remains critical during convection in a porous medium. This could be expected as an increase in σ is proportional to an increase in the solid phase percentage offering more volumetric resistance to the shearing action. At the same time a considerable uniform reduction in local fluid volume enhances local density differences responsible for the development of buoyancy force.

The stability curves of the basic motion in a wider gap ($R = 0.1$) on the (σ, Gr_c) plane is shown in Fig. 7 for various values of Pr_m. In general α stabilizes the base flow. We observe that fluids with larger Pr_m are less stable. The stability curve for $Pr_m = 4$ is qualitatively different from others. It has a cuspidal point near $\sigma = 3$

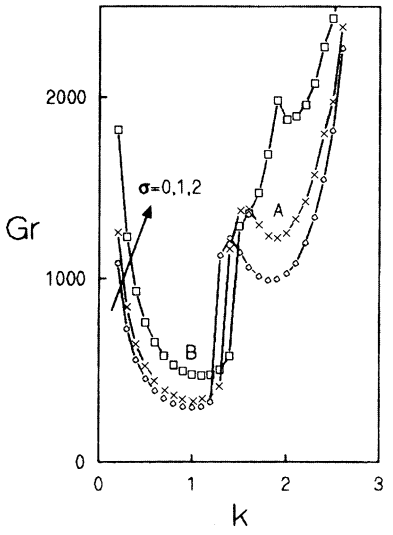

Fig. 5. Marginal stability curves for different σ when $\bar{\mu} = 1$, $R = 0.4$ and $Pr_m = 5$.

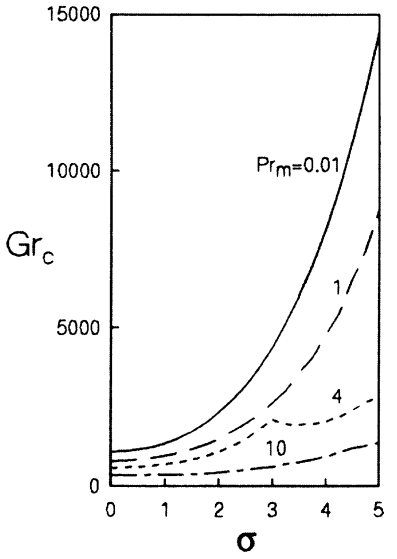

Fig. 7. Gr_c against σ for different Pr_m when $\bar{\mu} = 1$ and $R = 0.1$.

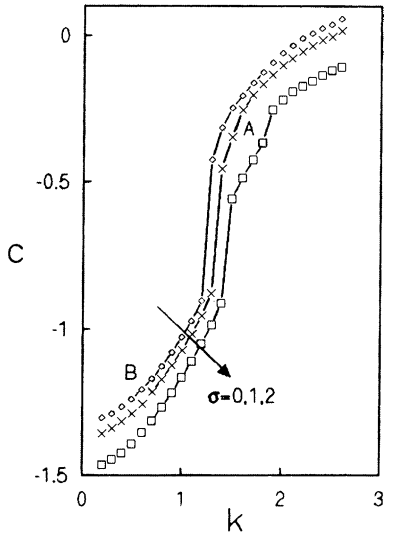

Fig. 6. Marginal wavespeeds for different σ when $\bar{\mu} = 1$, $R = 0.4$ and $Pr_m = 5$.

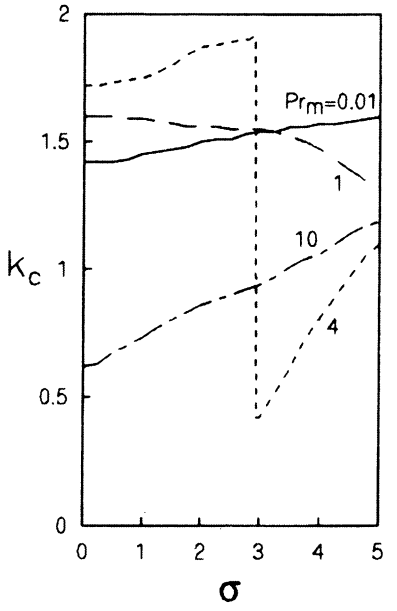

Fig. 8. k_c against σ for different Pr_m when $\bar{\mu} = 1$ and $R = 0.1$.

and this makes the flow unstable in the immediate neighbourhood $\sigma \in (3, 3.5)$ as σ increases. Some information on the secondary flow may be drawn from Figs. 8 and 9 displaying critical wavenumber k_c and critical wavespeed c_c. The transition from S to TB mode at $\sigma = 3$ for $Pr_m = 4$ is marked by jumps in both k_c and c_c. Physically this represents a sudden change in the vertical cell size. This abrupt change in the critical mechanism for $Pr_m = 4$ is shown in Fig. 10. We observe a sudden reduction in the S mode accompanied by a shift of the global minimum to the TB mode as σ increases from 2.75 to 3. Thus a critical TB mode is introduced by σ even for lower R. This is analogous to those arising in our previous result [20], where the basic state of convection in an inclined slot is induced by the combined effect of uniformly distributed heat sources and a moving sidewall. The perturbations begin to travel in the downward direction when Pr_m becomes 10 for all σ.

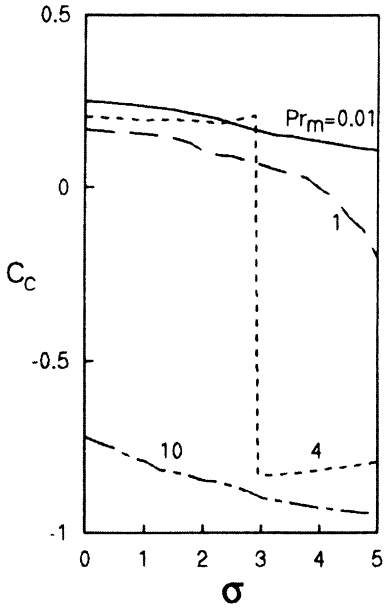

Fig. 9. c_c against σ for different Pr_m when $\bar{\mu} = 1$ and $R = 0.1$.

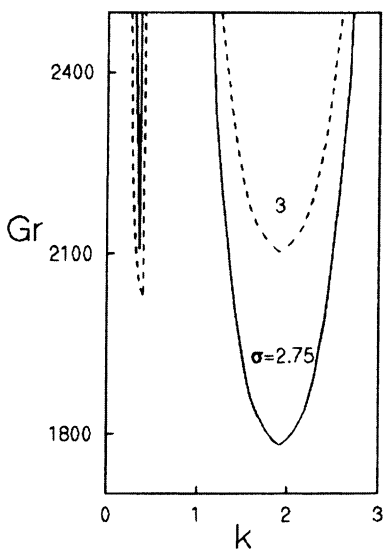

Fig. 10. Marginal stability curves near the change in critical mode.

Figs. 11–13 display the corresponding results for a medium gap, $R = 0.4$. We find that the vertical jump found for the case $R = 0.1$ is absent. Moreover, in contrast to $R = 0.1$, all the disturbances travel together with gravity.

As the radius ratio is found to alter the instability mechanism involved, we have plotted the stability characteristics against R in Figs. 14 and 15. We find that the effect of R is to stabilize the motion initially up to

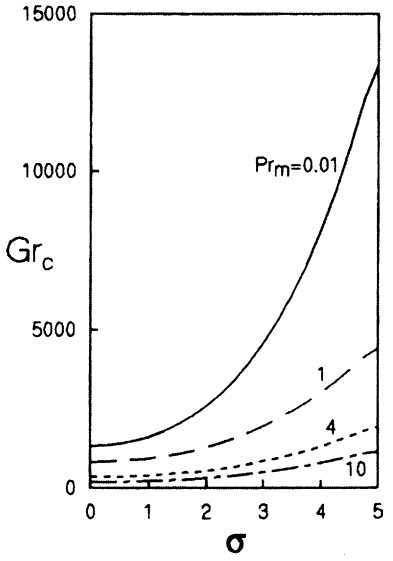

Fig. 11. Gr_c against σ for different Pr_m when $\bar{\mu} = 1$ and $R = 0.4$.

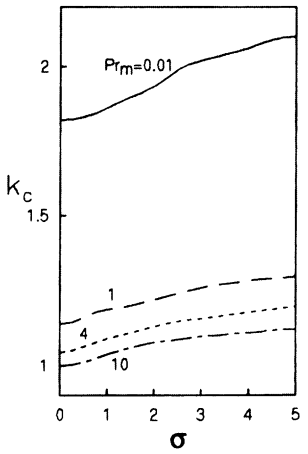

Fig. 12. k_c against σ for different Pr_m when $\bar{\mu} = 1$ and $R = 0.4$.

some values of R, depending on σ, and then destabilization becomes prominent for higher values of R. The critical curves undergo no substantial change and become nearly independent of R as the curvature becomes smaller. The corresponding wavespeeds show a sudden change in the direction of moving perturbations, in the form of thermal running waves for higher R. An increase in σ shifts the onset of instability due to the TB mode to smaller values of R. A comparison of the stability behaviour in a clear fluid ($\sigma = 0$) and a fluid saturated porous medium ($\sigma = 3$) is made in Figs. 16–19 against $Pr_m \in [0, 10]$, for various low values of R. This region of R is selected as it corresponds to sudden mode changing

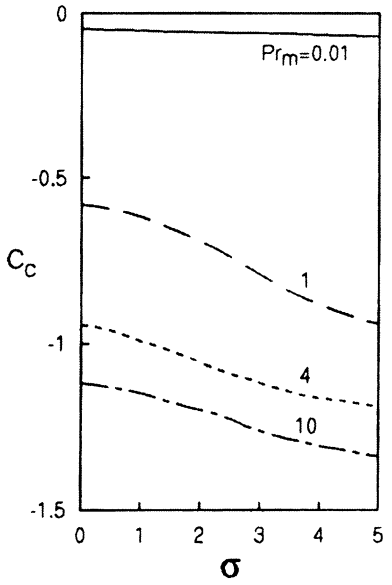

Fig. 13. c_c against σ for different Pr_m when $\bar{\mu} = 1$ and $R = 0.4$.

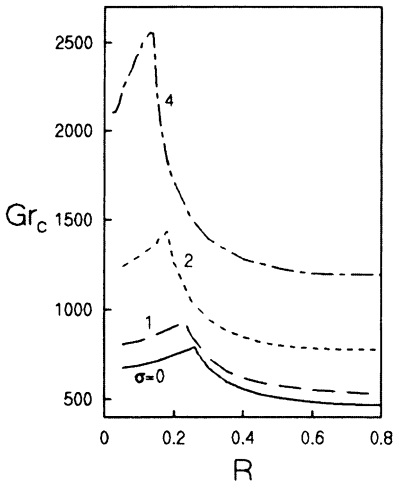

Fig. 14. Gr_c against R for different σ when $\bar{\mu} = 1$ and $Pr_m = 2$.

phenomena. We see that an increase in R speeds up the mode changing effect of Pr_m, as discussed earlier, when $\sigma = 3$ which is not felt when $\sigma = 0$. Moreover the two modes come closer and finally merge with each other, representing a continuous change from S to TB mode.

The effect of $\bar{\mu}$ on the critical boundaries are shown in Figs. 20 and 21. From these we infer that $\bar{\mu}$ stabilizes the system at a constant rate. The spacing between the cylinders with different $\bar{\mu}$ produces the same effect as discussed for Fig. 14.

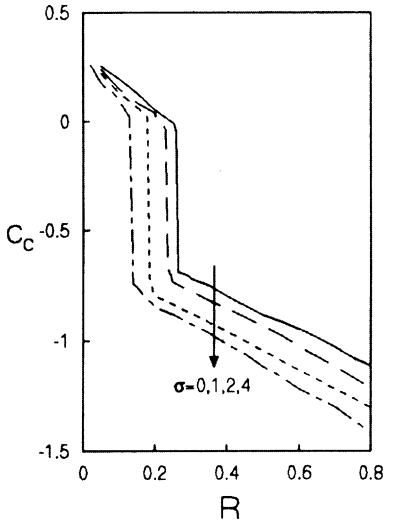

Fig. 15. c_c against R for different σ when $\bar{\mu} = 1$ and $Pr_m = 2$.

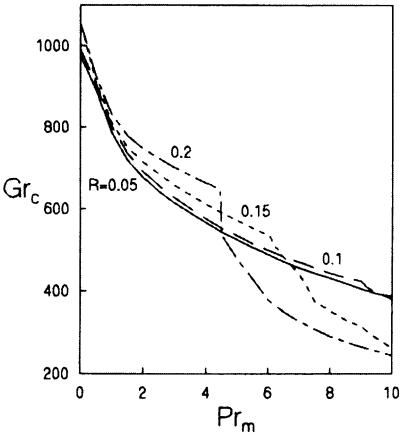

Fig. 16. Gr_c against Pr_m for different R when $\bar{\mu} = 1$ and $\sigma = 0$.

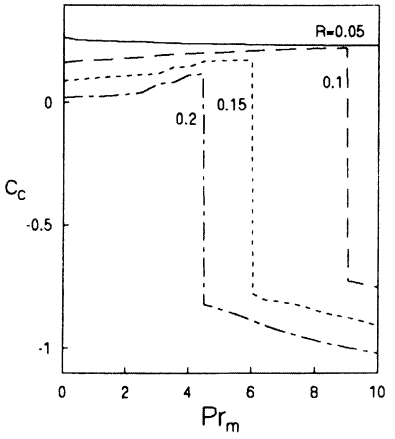

Fig. 17. c_c against Pr_m for different R when $\bar{\mu} = 1$ and $\sigma = 0$.

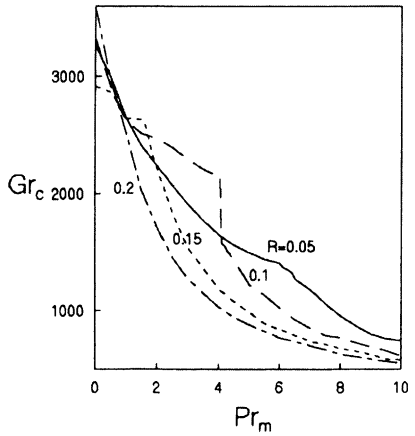

Fig. 18. Gr_c against Pr_m for different R when $\bar{\mu} = 1$ and $\sigma = 3$.

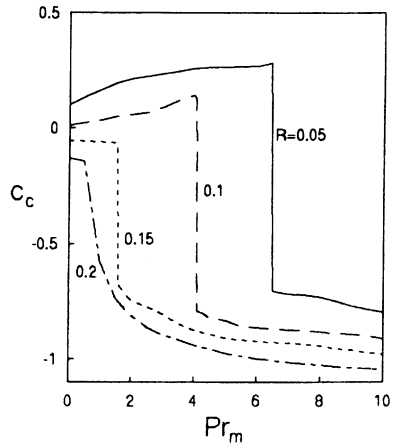

Fig. 19. c_c against Pr_m for different R when $\bar{\mu} = 1$ and $\sigma = 3$.

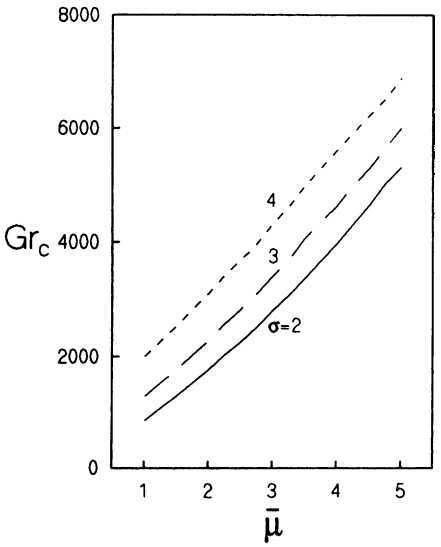

Fig. 20. Gr_c against $\bar{\mu}$ for different σ when $R = 0.4$ and $Pr_m = 2$.

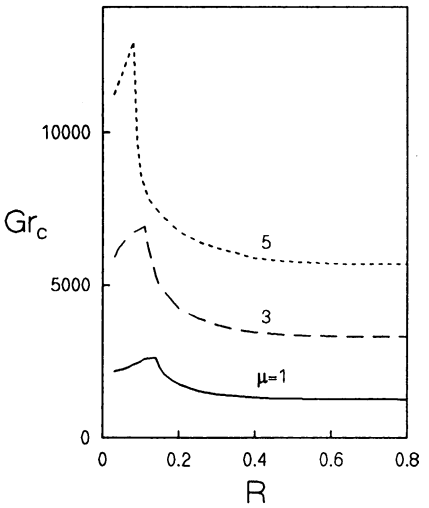

Fig. 21. Gr_c against R for different $\bar{\mu}$ when $\sigma = 3$ and $Pr_m = 2$.

5. Conclusion

A complete analysis for the stability of convection in an annular porous layer is done. In general σ makes the system more observable. The underlying critical mechanism is changed to TB mode by σ for lower R. The perturbations at the onset of instability always travel downward for higher R. R is also found to alter the basic mechanism for instability. At the same time, the effect of R is pronounced only in higher and medium gaps. Very low values of R are found to accelerate the mode changing effect of Pr_m. The critical curves in the $(\bar{\mu}, Gr_c)$ plane are found to be linear.

Acknowledgements

This work was done when the first author (S S) held a Senior Research Fellowship (NET) of CSIR, India.

Appendix A

The solution of the equation

$$\frac{d^2 v_0(r)}{dr^2} + \frac{1}{r}\frac{dv_0(r)}{dr} - \frac{G}{C} v_0(r) = G\left(D + \frac{r^2}{2} - A\log r - B\right)$$

where $G = 1/\bar{\mu}$ and $C = 1/\sigma^2$ with the boundary conditions $v_0(r_i) = 0$, $i = 1, 2$ is sought in the form $v_0(r) = \sum_{i=0}^{4} c_i (r - \bar{r})^i$.

The separation constant $D = dp_0/dr$ is

$$D = -\frac{d_1 + d_2 \log \bar{r}}{2\bar{r} d_3}$$

where

$$
\begin{aligned}
d_1 = {} & 2160AC^2\bar{r}^4r_1 - 1440BC^2\bar{r}^4r_1 - 275ACG\bar{r}^6r_1 \\
& + 60BCG\bar{r}^6r_1 + 135CG\bar{r}^8r_1 + 35AG^2\bar{r}^8r_1 \\
& - 60BG^2\bar{r}^8r_1 + 5G^2\bar{r}^{10}r_1 - 2048AC^2\bar{r}^3r_1^2 \\
& + 512ACG\bar{r}^5r_1^2 - 256CG\bar{r}^7r_1^2 - 96AG^2\bar{r}^7r_1^2 \\
& + 128BG^2\bar{r}^7r_1^2 + 504AC^2\bar{r}^2r_1^3 + 288BC^2\bar{r}^2r_1^3 \\
& + 360C^2\bar{r}^4r_1^3 - 279ACG\bar{r}^4r_1^3 - 144BCG\bar{r}^4r_1^3 \\
& + 165CG\bar{r}^6r_1^3 + 95AG^2\bar{r}^6r_1^3 - 96BG^2\bar{r}^6r_1^3 \\
& - 9G^2\bar{r}^8r_1^3 - 90BC^2\bar{r}r_1^4 - 135C^2\bar{r}^3r_1^4 \\
& + 40ACG\bar{r}^3r_1^4 + 60BCG\bar{r}^3r_1^4 - 30CG\bar{r}^5r_1^4 \\
& - 40AG^2\bar{r}^5r_1^4 + 30BG^2\bar{r}^5r_1^4 + 5G^2\bar{r}^7r_1^4 - 8AC^2r_1^5 \\
& + 24C^2\bar{r}^2r_1^5 + 2ACG\bar{r}^2r_1^5 - 12BCG\bar{r}^2r_1^5 + 8CG\bar{r}^4r_1^5 \\
& + 6AG^2\bar{r}^4r_1^5 - 4BG^2\bar{r}^4r_1^5 + 2160AC^2\bar{r}^4r_2 \\
& - 1440BC^2\bar{r}^4r_2 - 275ACG\bar{r}^6r_2 + 60BCG\bar{r}^6r_2 \\
& + 135CG\bar{r}^8r_2 + 35AG^2\bar{r}^8r_2 - 60BG^2\bar{r}^8r_2 \\
& + 5G^2\bar{r}^{10}r_2 - 3584AC^2\bar{r}^3r_1r_2 + 896ACG\bar{r}^5r_1r_2 \\
& - 448CG\bar{r}^7r_1r_2 - 168AG^2\bar{r}^7r_1r_2 + 224BG^2\bar{r}^7r_1r_2 \\
& + 1296AC^2\bar{r}^2r_1^2r_2 + 1152BC^2\bar{r}^2r_1^2r_2 + 720C^2\bar{r}^4r_1^2r_2 \\
& - 936ACG\bar{r}^4r_1^2r_2 - 216BCG\bar{r}^4r_1^2r_2 + 420CG\bar{r}^6r_1^2r_2 \\
& + 280AG^2\bar{r}^6r_1^2r_2 - 264BG^2\bar{r}^6r_1^2r_2 - 36G^2\bar{r}^8r_1^2r_2 \\
& - 360BC^2\bar{r}r_1^3r_2 - 540C^2\bar{r}^3r_1^3r_2 + 352ACG\bar{r}^3r_1^3r_2 \\
& + 240BCG\bar{r}^3r_1^3r_2 - 120CG\bar{r}^5r_1^3r_2 - 208AG^2\bar{r}^5r_1^3r_2 \\
& + 120BG^2\bar{r}^5r_1^3r_2 + 44G^2\bar{r}^7r_1^3r_2 - 32AC^2r_1^4r_2 \\
& + 96C^2\bar{r}^2r_1^4r_2 - 37ACG\bar{r}^2r_1^4r_2 - 48BCG\bar{r}^2r_1^4r_2 \\
& - 13CG\bar{r}^4r_1^4r_2 + 69AG^2\bar{r}^4r_1^4r_2 - 16BG^2\bar{r}^4r_1^4r_2 \\
& - 15G^2\bar{r}^6r_1^4r_2 - 8AG^2\bar{r}^3r_1^5r_2 - 2048AC^2\bar{r}^3r_2^2 \\
& + 512ACG\bar{r}^5r_2^2 - 256CG\bar{r}^7r_2^2 - 96AG^2\bar{r}^7r_2^2 \\
& + 128BG^2\bar{r}^7r_2^2 + 1296AC^2\bar{r}^2r_1r_2^2 + 1152BC^2\bar{r}^2r_1r_2^2 \\
& + 720C^2\bar{r}^4r_1r_2^2 - 936ACG\bar{r}^4r_1r_2^2 - 216BCG\bar{r}^4r_1r_2^2 \\
& + 420CG\bar{r}^6r_1r_2^2 + 280AG^2\bar{r}^6r_1r_2^2 - 264BG^2\bar{r}^6r_1r_2^2 \\
& - 36G^2\bar{r}^8r_1r_2^2 - 540BC^2\bar{r}r_1^2r_2^2 - 810C^2\bar{r}^3r_1^2r_2^2 \\
& + 496ACG\bar{r}^3r_1^2r_2^2 + 360BCG\bar{r}^3r_1^2r_2^2 - 180CG\bar{r}^5r_1^2r_2^2 \\
& - 304AG^2\bar{r}^5r_1^2r_2^2 + 180BG^2\bar{r}^5r_1^2r_2^2 + 62G^2\bar{r}^7r_1^2r_2^2 \\
& - 80AC^2r_1^3r_2^2 + 240C^2\bar{r}^2r_1^3r_2^2 - 70ACG\bar{r}^2r_1^3r_2^2 \\
& - 120BCG\bar{r}^2r_1^3r_2^2 - 10CG\bar{r}^4r_1^3r_2^2 + 150AG^2\bar{r}^4r_1^3r_2^2 \\
& - 40BG^2\bar{r}^4r_1^3r_2^2 - 30G^2\bar{r}^6r_1^3r_2^2 - 32AG^2\bar{r}^3r_1^4r_2^2 \\
& - 2ACGr_1^5r_2^2 + 6CG\bar{r}^2r_1^5r_2^2 + 2AG^2\bar{r}^2r_1^5r_2^2 + 2G^2\bar{r}^4r_1^5r_2^2 \\
& + 504AC^2\bar{r}^2r_2^3 + 288BC^2\bar{r}^2r_2^3 + 360C^2\bar{r}^4r_2^3 \\
& - 279ACG\bar{r}^4r_2^3 - 144BCG\bar{r}^4r_2^3 + 165CG\bar{r}^6r_2^3 \\
& + 95AG^2\bar{r}^6r_2^3 - 96BG^2\bar{r}^6r_2^3 - 9G^2\bar{r}^8r_2^3 - 360BC^2\bar{r}r_1r_2^3 \\
& - 540C^2\bar{r}^3r_1r_2^3 + 352ACG\bar{r}^3r_1r_2^3 + 240BCG\bar{r}^3r_1r_2^3 \\
& - 120CG\bar{r}^5r_1r_2^3 - 208AG^2\bar{r}^5r_1r_2^3 + 120BG^2\bar{r}^5r_1r_2^3 \\
& + 44G^2\bar{r}^7r_1r_2^3 - 80AC^2r_1^2r_2^3 + 240C^2\bar{r}^2r_1^2r_2^3 \\
& - 70ACG\bar{r}^2r_1^2r_2^3 - 120BCG\bar{r}^2r_1^2r_2^3 - 10CG\bar{r}^4r_1^2r_2^3 \\
& + 150AG^2\bar{r}^4r_1^2r_2^3 - 40BG^2\bar{r}^4r_1^2r_2^3 - 30G^2\bar{r}^6r_1^2r_2^3 \\
& - 40AG^2\bar{r}^3r_1^3r_2^3 - 3ACGr_1^4r_2^3 + 9CG\bar{r}^2r_1^4r_2^3 \\
& + 3AG^2\bar{r}^2r_1^4r_2^3 + 3G^2\bar{r}^4r_1^4r_2^3 - 90BC^2\bar{r}r_2^4 - 135C^2\bar{r}^3r_2^4 \\
& + 40ACG\bar{r}^3r_2^4 + 60BCG\bar{r}^3r_2^4 - 30CG\bar{r}^5r_2^4 \\
& - 40AG^2\bar{r}^5r_2^4 + 30BG^2\bar{r}^5r_2^4 + 5G^2\bar{r}^7r_2^4 - 32AC^2r_1r_2^4 \\
& + 96C^2\bar{r}^2r_1r_2^4 - 37ACG\bar{r}^2r_1r_2^4 - 48BCG\bar{r}^2r_1r_2^4 \\
& - 13CG\bar{r}^4r_1r_2^4 + 69AG^2\bar{r}^4r_1r_2^4 - 16BG^2\bar{r}^4r_1r_2^4 \\
& - 15G^2\bar{r}^6r_1r_2^4 - 32AG^2\bar{r}^3r1^2r_2^4 - 3ACGr_1^3r_2^4 \\
& + 9CG\bar{r}^2r_1^3r_2^4 + 3AG^2\bar{r}^2r_1^3r_2^4 + 3G^2\bar{r}^4r_1^3r_2^4 - 8AC^2r_2^5 \\
& + 24C^2\bar{r}^2r_2^5 + 2ACG\bar{r}^2r_2^5 - 12BCG\bar{r}^2r_2^5 + 8CG\bar{r}^4r_2^5 \\
& + 6AG^2\bar{r}^4r_2^5 - 4BG^2\bar{r}^4r_2^5 - 8AG^2\bar{r}^3r_1r_2^5 - 2ACGr_1^2r_2^5 \\
& + 6CG\bar{r}^2r_1^2r_2^5 + 2AG^2\bar{r}^2r_1^2r_2^5 + 2G^2\bar{r}^4r_1^2r_2^5
\end{aligned}
$$

$$
\begin{aligned}
d_2 = {} & -1440AC^2\bar{r}^4r_1 + 60ACG\bar{r}^6r_1 - 60AG^2\bar{r}^8r_1 \\
& + 128AG^2\bar{r}^7r_1^2 + 288AC^2\bar{r}^2r_1^3 - 144ACG\bar{r}^4r_1^3 \\
& - 96AG^2\bar{r}^6r_1^3 - 90AC^2\bar{r}r_1^4 + 60ACG\bar{r}^3r_1^4 + 30AG^2\bar{r}^5r_1^4 \\
& - 12ACG\bar{r}^2r_1^5 - 4AG^2\bar{r}^4r_1^5 - 1440AC^2\bar{r}^4r_2 \\
& + 60ACG\bar{r}^6r_2 - 60AG^2\bar{r}^8r_2 + 224AG^2\bar{r}^7r_1r_2 \\
& + 1152AC^2\bar{r}^2r_1^2r_2 - 216ACG\bar{r}^4r_1^2r_2 - 264AG^2\bar{r}^6r_1^2r_2 \\
& - 360AC^2\bar{r}r_1^3r_2 + 240ACG\bar{r}^3r_1^3r_2 + 120AG^2\bar{r}^5r_1^3r_2 \\
& - 48ACG\bar{r}^2r_1^4r_2 - 16AG^2\bar{r}^4r_1^4r_2 + 128AG^2\bar{r}^7r_2^2 \\
& + 1152AC^2\bar{r}^2r_1r_2^2 - 216ACG\bar{r}^4r_1r_2^2 - 264AG^2\bar{r}^6r_1r_2^2 \\
& - 540AC^2\bar{r}r_1^2r_2^2 + 360ACG\bar{r}^3r_1^2r_2^2 + 180AG^2\bar{r}^5r_1^2r_2^2 \\
& - 120ACG\bar{r}^2r_1^3r_2^2 - 40AG^2\bar{r}^4r_1^3r_2^2 + 288AC^2\bar{r}^2r_2^3 \\
& - 144ACG\bar{r}^4r_2^3 - 96AG^2\bar{r}^6r_2^3 - 360AC^2\bar{r}r_1r_2^3 \\
& + 240ACG\bar{r}^3r_1r_2^3 + 120AG^2\bar{r}^5r_1r_2^3 - 120ACG\bar{r}^2r_1^2r_2^3 \\
& - 40AG^2\bar{r}^4r_1^2r_2^3 - 90AC^2\bar{r}r_2^4 + 60ACG\bar{r}^3r_2^4 \\
& + 30AG^2\bar{r}^5r_2^4 - 48ACG\bar{r}^2r_1r_2^4 - 16AG^2\bar{r}^4r_1r_2^4 \\
& - 12ACG\bar{r}^2r_2^5 - 4AG^2\bar{r}^4r_2^5
\end{aligned}
$$

$$
\begin{aligned}
d_3 = {} & 720C^2\bar{r}^3r_1 - 30CG\bar{r}^5r_1 + 30G^2\bar{r}^7r_1 - 64G^2\bar{r}^6r_1^2 \\
& - 144C^2\bar{r}r_1^3 + 72CG\bar{r}^3r_1^3 + 48G^2\bar{r}^5r_1^3 + 45C^2r_1^4 \\
& - 30CG\bar{r}^2r_1^4 - 15G^2\bar{r}^4r_1^4 + 6CG\bar{r}r_1^5 + 2G^2\bar{r}^3r_1^5 \\
& + 720C^2\bar{r}^3r_2 - 30CG\bar{r}^5r_2 + 30G^2\bar{r}^7r_2 - 112G^2\bar{r}^6r_1r_2 \\
& - 576C^2\bar{r}r_1^2r_2 + 108CG\bar{r}^3r_1^2r_2 + 132G^2\bar{r}^5r_1^2r_2 \\
& + 180C^2r_1^3r_2 - 120CG\bar{r}^2r_1^3r_2 - 60G^2\bar{r}^4r_1^3r_2 \\
& + 24CG\bar{r}r_1^4r_2 + 8G^2\bar{r}^3r_1^4r_2 - 64G^2\bar{r}^6r_2^2 - 576C^2\bar{r}r_1r_2^2 \\
& + 108CG\bar{r}^3r_1r_2^2 + 132G^2\bar{r}^5r_1r_2^2 + 270C^2r_1^2r_2^2 \\
& - 180CG\bar{r}^2r_1^2r_2^2 - 90G^2\bar{r}^4r_1^2r_2^2 + 60CG\bar{r}r_1^3r_2^2 \\
& + 20G^2\bar{r}^3r_1^3r_2^2 - 144C^2\bar{r}r_2^3 + 72CG\bar{r}^3r_2^3 + 48G^2\bar{r}^5r_2^3 \\
& + 180C^2r_1r_2^3 - 120CG\bar{r}^2r_1r_2^3 - 60G^2\bar{r}^4r_1r_2^3 \\
& + 60CG\bar{r}r_1^2r_2^3 + 20G^2\bar{r}^3r_1^2r_2^3 + 45C^2r_2^4 - 30CG\bar{r}^2r_2^4 \\
& - 15G^2\bar{r}^4r_2^4 + 24CG\bar{r}r_1r_2^4 + 8G^2\bar{r}^3r_1r_2^4 + 6CG\bar{r}r_2^5 \\
& + 2G^2\bar{r}^3r_2^5
\end{aligned}
$$

The coefficients c_i's are given by

$$c_0 = -\frac{CG(r_1-\bar{r})(r_2-\bar{r})(c_{01}+c_{02}\log\bar{r})}{2\bar{r}c_{03}}$$

where

$$\begin{aligned}
c_{01} = {} & 212AC^2\bar{r}^4 - 288BC^2\bar{r}^4 + 288DC^2\bar{r}^4 + 36C^2\bar{r}^6 \\
& - 6BCG\bar{r}^6 + 6DCG\bar{r}^6 + 7CG\bar{r}^8 - 2BG^2\bar{r}^8 + 2DG^2\bar{r}^8 \\
& + G^2\bar{r}^{10} - 172AC^2\bar{r}^3r_1 + 78BC^2\bar{r}^3r_1 - 78DC^2\bar{r}^3r_1 \\
& + 9C^2\bar{r}^5r_1 + 6BCG\bar{r}^5r_1 - 6DCG\bar{r}^5r_1 - 11CG\bar{r}^7r_1 \\
& + 4BG^2\bar{r}^7r_1 - 4DG^2\bar{r}^7r_1 - 2G^2\bar{r}^9r_1 + 32AC^2\bar{r}^2r_1^2 \\
& - 18BC^2\bar{r}^2r_1^2 + 18DC^2\bar{r}^2r_1^2 + 21C^2\bar{r}^4r_1^2 \\
& - 12BCG\bar{r}^4r_1^2 + 12DCG\bar{r}^4r_1^2 + 10CG\bar{r}^6r_1^2 \\
& - 2BG^2\bar{r}^6r_1^2 + 2DG^2\bar{r}^6r_1^2 + G^2\bar{r}^8r_1^2 - 172AC^2\bar{r}^3r_2 \\
& + 78BC^2\bar{r}^3r_2 - 78DC^2\bar{r}^3r_2 + 9C^2\bar{r}^5r_2 + 6BCG\bar{r}^5r_2 \\
& - 6DCG\bar{r}^5r_2 - 11CG\bar{r}^7r_2 + 4BG^2\bar{r}^7r_2 - 4DG^2\bar{r}^7r_2 \\
& - 2G^2\bar{r}^9r_2 + 80AC^2\bar{r}^2r_1r_2 + 60BC^2\bar{r}^2r_1r_2 \\
& - 60DC^2\bar{r}^2r_1r_2 - 6C^2\bar{r}^4r_1r_2 + 12BCG\bar{r}^4r_1r_2 \\
& - 12DCG\bar{r}^4r_1r_2 + 10CG\bar{r}^6r_1r_2 - 8BG^2\bar{r}^6r_1r_2 \\
& + 8DG^2\bar{r}^6r_1r_2 + 4G^2\bar{r}^8r_1r_2 - 4AC^2\bar{r}r_1^2r_2 \\
& - 18BC^2\bar{r}r_1^2r_2 + 18DC^2\bar{r}r_1^2r_2 - 15C^2\bar{r}^3r_1^2r_2 \\
& + 6BCG\bar{r}^3r_1^2r_2 - 6DCG\bar{r}^3r_1^2r_2 - 11CG\bar{r}^5r_1^2r_2 \\
& + 4BG^2\bar{r}^5r_1^2r_2 - 4DG^2\bar{r}^5r_1^2r_2 - 2G^2\bar{r}^7r_1^2r_2 \\
& + 32AC^2\bar{r}^2r_2^2 - 18BC^2\bar{r}^2r_2^2 + 18DC^2\bar{r}^2r_2^2 + 21C^2\bar{r}^4r_2^2 \\
& - 12BCG\bar{r}^4r_2^2 + 12DCG\bar{r}^4r_2^2 + 10CG\bar{r}^6r_2^2 \\
& - 2BG^2\bar{r}^6r_2^2 + 2DG^2\bar{r}^6r_2^2 + G^2\bar{r}^8r_2^2 - 4AC^2\bar{r}r_1r_2^2 \\
& - 18BC^2\bar{r}r_1r_2^2 + 18DC2\bar{r}r_1r_2^2 - 15C^2\bar{r}^3r_1r_2^2 \\
& + 6BCG\bar{r}^3r_1r_2^2 - 6DCG\bar{r}^3r_1r_2^2 - 11CG\bar{r}^5r_1r_2^2 \\
& + 4BG^2\bar{r}^5r_1r_2^2 - 4DG^2\bar{r}^5r_1r_2^2 - 2G^2\bar{r}^7r_1r_2^2 \\
& - 4AC^2r_1^2r_2^2 + 12C^2\bar{r}^2r_1^2r_2^2 - 6BCG\bar{r}^2r_1^2r_2^2 \\
& + 6DCG\bar{r}^2r_1^2r_2^2 + 7CG\bar{r}^4r_1^2r_2^2 - 2BG^2\bar{r}^4r_1^2r_2^2 \\
& + 2DG^2\bar{r}^4r_1^2r_2^2 + G^2\bar{r}^6r_1^2r_2^2
\end{aligned}$$

$$\begin{aligned}
c_{02} = {} & -288AC^2\bar{r}^4 - 6ACG\bar{r}^6 - 2AG^2\bar{r}^8 + 78AC^2\bar{r}^3r_1 \\
& + 6ACG\bar{r}^5r_1 + 4AG^2\bar{r}^7r_1 - 18AC^2\bar{r}^2r_1^2 - 12ACG\bar{r}^4r_1^2 \\
& - 2AG^2\bar{r}^6r_1^2 + 78AC^2\bar{r}^3r_2 + 6ACG\bar{r}^5r_2 + 4AG^2\bar{r}^7r_2 \\
& + 60AC^2\bar{r}^2r_1r_2 + 12ACG\bar{r}^4r_1r_2 - 8AG^2\bar{r}^6r_1r_2 \\
& - 18AC^2\bar{r}r_1^2r_2 + 6ACG\bar{r}^3r_1^2r_2 + 4AG^2\bar{r}^5r_1^2r_2 \\
& - 18AC^2\bar{r}^2r_2^2 - 12ACG\bar{r}^4r_2^2 - 2AG^2\bar{r}^6r_2^2 \\
& - 18AC^2\bar{r}r_1r_2^2 + 6ACG\bar{r}^3r_1r_2^2 + 4AG^2\bar{r}^5r_1r_2^2 \\
& - 6ACG\bar{r}^2r_1^2r_2^2 - 2AG^2\bar{r}^4r_1^2r_2^2
\end{aligned}$$

$$\begin{aligned}
c_{03} = {} & -576C^3\bar{r}^3 + 24C^2G\bar{r}^5 + 3CG^2\bar{r}^7 + G^3\bar{r}^9 \\
& + 432C^3\bar{r}^2r_1 - 39C^2G\bar{r}^4r_1 - 6CG^2\bar{r}^6r_1 - 3G^3\bar{r}^8r_1 \\
& - 192C^3\bar{r}r_1^2 - 24C^2G\bar{r}^3r_1^2 + 9CG^2\bar{r}^5r_1^2 + 3G^3\bar{r}^7r_1^2 \\
& + 36C^3r_1^3 + 3C^2G\bar{r}^2r_1^3 - 6CG^2\bar{r}^4r_1^3 - G^3\bar{r}^6r_1^3 \\
& + 432C^3\bar{r}^2r_2 - 39C^2G\bar{r}^4r_2 - 6CG^2\bar{r}^6r_2 - 3G^3\bar{r}8r_2 \\
& - 192C^3\bar{r}r_1r_2 + 120C^2G\bar{r}^3r_1r_2 + 3CG^2\bar{r}5r_1r_2 \\
& + 9G^3\bar{r}^7r_1r_2 + 36C^3r_1^2r_2 + 3C^2G\bar{r}^2r_1^2r_2 - 6CG^2\bar{r}^4r_1^2r_2 \\
& - 9G^3\bar{r}^6r_1^2r_2 + 9CG^2\bar{r}^3r_1^3r_2 + 3G^3\bar{r}^5r_1^3r_2 - 192C^3\bar{r}r_2^2 \\
& - 24C^2G\bar{r}^3r_2^2 + 9CG^2\bar{r}^5r_2^2 + 3G^3\bar{r}^7r_2^2 + 36C^3r_1r_2^2 \\
& + 3C^2G\bar{r}^2r_1r_2^2 - 6CG^2\bar{r}^4r_1r_2^2 - 9G^3\bar{r}^6r_1r_2^2 \\
& - 48C^2G\bar{r}r_1^2r_2^2 + 3CG^2\bar{r}^3r_1^2r_2^2 + 9G^3\bar{r}^5r_1^2r_2^2 \\
& + 9C^2Gr_1^3r_2^2 - 6CG^2\bar{r}^2r_1^3r_2^2 - 3G^3\bar{r}^4r_1^3r_2^2 + 36C^3r_2^3 \\
& + 3C^2G\bar{r}^2r_2^3 - 6CG^2\bar{r}^4r_2^3 - G^3\bar{r}^6r_2^3 + 9CG^2\bar{r}^3r_1r_2^3 \\
& + 3G^3\bar{r}^5r_1r_2^3 + 9C^2Gr_1^2r_2^3 - 6CG^2\bar{r}^2r_1^2r_2^3 - 3G^3\bar{r}^4r_1^2r_2^3 \\
& + 3CG^2\bar{r}r_1^3r_2^3 + G^3\bar{r}^3r_1^3r_2^3
\end{aligned}$$

$$c_1 = \frac{CG(c_{04}+c_{05}\log\bar{r})}{c_{03}}$$

where

$$\begin{aligned}
c_{04} = {} & -120AC^2\bar{r}^4 + 288BC^2\bar{r}^4 - 288DC^2\bar{r}^4 - 72C^2\bar{r}^6 \\
& - 23ACG\bar{r}^6 + 24BCG\bar{r}^6 - 24DCG\bar{r}^6 - 3CG\bar{r}^8 \\
& + AG^2\bar{r}^8 - G^2\bar{r}^{10} + 144AC^2\bar{r}^3r_1 - 252BC^2\bar{r}^3r_1 \\
& + 252DC^2\bar{r}^3r_1 + 54C^2\bar{r}^5r_1 + 51ACG\bar{r}^5r_1 \\
& - 36BCG\bar{r}^5r_1 + 36DCG\bar{r}^5r_1 + 3CG\bar{r}^7r_1 \\
& - 3AG^2\bar{r}^7r_1 + 3G^2\bar{r}^9r_1 - 72AC^2\bar{r}^2r_1^2 + 96BC^2\bar{r}^2r_1^2 \\
& - 96DC^2\bar{r}^2r_1^2 - 24C^2\bar{r}^4r_1^2 - 33ACG\bar{r}^4r_1^2 \\
& + 24BCG\bar{r}^4r_1^2 - 24DCG\bar{r}^4r_1^2 - 9CG\bar{r}^6r_1^2 + 3AG^2\bar{r}^6r_1^2 \\
& - 3G^2\bar{r}^8r_1^2 + 12AC^2\bar{r}r_1^3 - 18BC^2\bar{r}r_1^3 + 18DC^2\bar{r}r_1^3 \\
& + 9C^2\bar{r}^3r_1^3 + 5ACG\bar{r}^3r_1^3 - 6BCG\bar{r}^3r_1^3 + 6DCG\bar{r}^3r_1^3 \\
& + 6CG\bar{r}^5r_1^3 - AG^2\bar{r}^5r_1^3 + G^2\bar{r}^7r_1^3 + 144AC^2\bar{r}^3r_2 \\
& - 252BC^2\bar{r}^3r_2 + 252DC^2\bar{r}^3r_2 + 54C^2\bar{r}^5r_2 \\
& + 51ACG\bar{r}^5r_2 - 36BCG\bar{r}^5r_2 + 36DCG\bar{r}^5r_2 \\
& + 3CG\bar{r}^7r_2 - 3AG^2\bar{r}^7r_2 + 3G^2\bar{r}^9r_2 - 72AC^2\bar{r}^2r_1r_2 \\
& + 96BC^2\bar{r}^2r_1r_2 - 96DC^2\bar{r}^2r_1r_2 - 24C^2\bar{r}^4r_1r_2 \\
& - 111ACG\bar{r}^4r_1r_2 + 24BCG\bar{r}^4r_1r_2 - 24DCG\bar{r}^4r_1r_2 \\
& + 9CG\bar{r}^6r_1r_2 + 9AG^2\bar{r}^6r_1r_2 - 9G^2\bar{r}^8r_1r_2 \\
& + 12AC^2\bar{r}r_1^2r_2 - 18BC^2\bar{r}r_1^2r_2 + 18DC^2\bar{r}r_1^2r_2 \\
& + 9C^2\bar{r}^3r_1^2r_2 + 69ACG\bar{r}^3r_1^2r_2 - 6BCG\bar{r}^3r_1^2r_2 \\
& + 6DCG\bar{r}^3r_1^2r_2 + 6CG\bar{r}^5r_1^2r_2 - 9AG^2\bar{r}^5r_1^2r_2 \\
& + 9G^2\bar{r}^7r_1^2r_2 - 9ACG\bar{r}^2r_1^3r_2 - 9CG\bar{r}^4r_1^3r_2 \\
& + 3AG^2\bar{r}^4r_1^3r_2 - 3G^2\bar{r}^6r_1^3r_2 - 72AC^2\bar{r}^2r_2^2 + 96BC^2\bar{r}^2r_2^2 \\
& - 96DC^2\bar{r}^2r_2^2 - 24C^2\bar{r}^4r_2^2 - 33ACG\bar{r}^4r_2^2 + 24BCG\bar{r}^4r_2^2
\end{aligned}$$

$$
\begin{aligned}
&- 24DCG\bar{r}^4r_2^2 - 9CG\bar{r}^6r_2^2 + 3AG^2\bar{r}^6r_2^2 - 3G^2\bar{r}^8r_2^2\\
&+ 12AC^2\bar{r}r_1r_2^2 - 18BC^2\bar{r}r_1r_2^2 + 18DC^2\bar{r}r_1r_2^2\\
&+ 9C^2\bar{r}^3r_1r_2^2 + 69ACG\bar{r}^3r_1r_2^2 - 6BCG\bar{r}^3r_1r_2^2\\
&+ 6DCG\bar{r}^3r_1r_2^2 + 6CG\bar{r}^5r_1r_2^2 - 9AG^2\bar{r}^5r_1r_2^2\\
&+ 9G^2\bar{r}^7r_1r_2^2 - 39ACG\bar{r}^2r_1^2r_2^2 - 15CG\bar{r}^4r_1^2r_2^2\\
&+ 9AG^2\bar{r}^4r_1^2r_2^2 - 9G^2\bar{r}^6r_1^2r_2^2 + 3ACG\bar{r}r_1^3r_2^2 + 9CG\bar{r}^3r_1^3r_2^2\\
&- 3AG^2\bar{r}^3r_1^3r_2^2 + 3G^2\bar{r}^5r_1^3r_2^2 + 12AC^2\bar{r}r_2^3 - 18BC^2\bar{r}r_2^3\\
&+ 18DC^2\bar{r}r_2^3 + 9C^2\bar{r}^3r_2^3 + 5ACG\bar{r}^3r_2^3 - 6BCG\bar{r}^3r_2^3\\
&+ 6DCG\bar{r}^3r_2^3 + 6CG\bar{r}^5r_2^3 - AG^2\bar{r}^5r_2^3 + G^2\bar{r}^7r_2^3\\
&- 9ACG\bar{r}^2r_1r_2^3 - 9CG\bar{r}^4r_1r_2^3 + 3AG^2\bar{r}^4r_1r_2^3\\
&- 3G^2\bar{r}^6r_1r_2^3 + 3ACG\bar{r}r_1^2r_2^3 + 9CG\bar{r}^3r_1^2r_2^3 - 3AG^2\bar{r}^3r_1^2r_2^3\\
&+ 3G^2\bar{r}^5r_1^2r_2^3 + ACGr_1^3r_2^3 - 3CG\bar{r}^2r_1^3r_2^3 + AG^2\bar{r}^2r_1^3r_2^3\\
&- G^2\bar{r}^4r_1^3r_2^3
\end{aligned}
$$

$$
\begin{aligned}
c_{05} = {} & 288AC^2\bar{r}^4 + 24ACG\bar{r}^6 - 252AC^2\bar{r}^3r_1 - 36ACG\bar{r}^5r_1\\
&+ 96AC^2\bar{r}^2r_1^2 + 24ACG\bar{r}^4r_1^2 - 18AC^2\bar{r}r_1^3 - 6ACG\bar{r}^3r_1^3\\
&- 252AC^2\bar{r}^3r_2 - 36ACG\bar{r}^5r_2 + 96AC^2\bar{r}^2r_1r_2\\
&+ 24ACG\bar{r}^4r_1r_2 - 18AC^2\bar{r}r_1^2r_2 - 6ACG\bar{r}^3r_1^2r_2\\
&+ 96AC^2\bar{r}^2r_2^2 + 24ACG\bar{r}^4r_2^2 - 18AC^2\bar{r}r_1r_2^2\\
&- 6ACG\bar{r}^3r_1r_2^2 - 18AC^2\bar{r}r_2^3 - 6ACG\bar{r}^3r_2^3
\end{aligned}
$$

$$c_2 = \frac{-BG}{2} + \frac{DG}{2} + \frac{a_0G}{2C} - \frac{a_1}{2\bar{r}} + \frac{G\bar{r}^2}{4} - \frac{AG\log\bar{r}}{2}$$

$$c_3 = \frac{a_1G}{6C} + \frac{a_1}{6\bar{r}^2} - \frac{a_2}{3\bar{r}} - \frac{AG}{6\bar{r}} + \frac{G\bar{r}}{6}$$

$$c_4 = \frac{G}{24} + \frac{a_2G}{12C} - \frac{a_1}{12\bar{r}^3} + \frac{a_2}{6\bar{r}^2} + \frac{AG}{24\bar{r}^2} - \frac{a_3}{4\bar{r}}$$

References

[1] A.I. VanHeek, Increasing the power of the high temperature reactor module, Nucl. Eng. Des. 150 (1994) 183–189.

[2] T.C. Chawla, D.R. Pedersen, W.J. Minkowycz, Governing equations for heat and mass transfer in heat generating porous beds. Part I: Coolant boiling and transient void propagation, Int. J. Heat Mass Transfer 28 (1985) 2129–2136.

[3] T.C. Chawla, D.R. Pedersen, W.J. Minkowycz, Governing equations for heat and mass transfer in heat generating porous beds. Part II: Particulate melting and substrate penetration by dissolution, Int. J. Heat Mass Transfer 28 (1985) 2137–2148.

[4] K.R. Westerterp, W.P.M. VanSwaaji, A.A.C.M. Beenackers, Chemical Reactor Design and Operation, Wiley, New York, 1984.

[5] V.Z. Yakhnin, A.B. Rovinsky, M. Menzinger, Convective instability induced by differential transport in the tubular packed-bed reactor, Chem. Eng. Sci. 50 (1995) 2853–2859.

[6] E.R. Lapwood, Convection of a fluid in a porous medium, Proc. Camb. Phil. Soc. 44 (1948) 508–521.

[7] K. Vafai, C.L. Tien, Boundary and inertia effects on flow and heat transfer in porous media, Int. J. Heat Mass Transfer 24 (1981) 195–203.

[8] H.C. Brinkman, A calculation of the viscous force exerted by a flowing fluid on a dense swarm of particles, Appl. Sci. Res. A 1 (1947) 27–34.

[9] D.A. Nield, A. Bejan, Convection in Porous Media, Springer, New York, 1999.

[10] W.E. Stewart, C.L.G. Dona, Free convection in a heat generating porous medium in a finite vertical cylinder, Trans. ASME—J. Heat Transfer 110 (1988) 517–520.

[11] V. Prasad, A. Chui, Natural convection in a cylindrical porous enclosure with internal heat generation, Trans. ASME—J. Heat Transfer 111 (1989) 916–925.

[12] W.W. Farr, J. Gabitto, D. Luss, V. Balakotaiah, Reaction-driven convection in a porous medium, AIChE J. 37 (1991) 963–985.

[13] P. Vassuer, T.H. Nguyen, L. Robillard, V.K.T. Thi, Natural convection between horizontal concentric cylinders filled with a porous layer with internal heat generation, Int. J. Heat Mass Transfer 27 (1984) 337–349.

[14] W.E. Stewart, A.S. Burns, Convection in a concentric annulus with heat generating porous media and permeable inner boundary, Int. Comm. Heat Mass Transfer 19 (1992) 859–868.

[15] P. Adnani, I. Catton, M.A. Abdou, Non-Darican forced convection in porous media with anisotropic dispersion, Trans. ASME—J. Heat Transfer 117 (1995) 447–451.

[16] V.M. Shikhov, V.I. Yakushin, Perm Pedagogical Institute, Perm 3 (1977) 140–144.

[17] A.A. Kolyshkin, R. Vaillancourt, Linear stability of Couette flow with rotating inner cylinder and radially nonuniform internal heat sources, Int. J. Heat Mass Transfer 39 (1996) 537–545.

[18] S. Thangam, C.F. Chen, Stability analysis on the convection of a variable viscosity fluid in an infinite vertical slot, Phys. Fluids 29 (1986) 1367–1372.

[19] G.Z. Gershuni, E.M. Zhukhovitskii, A.A. Iakimov, Two kinds of instability of stationary convective motion induced by internal heat sources, Prikl. Mat. Mekh. 37 (1973) 564–568.

[20] S. Saravanan, P. Kandaswamy, Stability of natural convective motion in pure water near 4 °C contained in a slot with a moving sidewall, Int. J. Heat Mass Transfer 45 (2002) 1321–1332.